Construction and Building Materials 164 (2018) 716–730

Contents lists available at ScienceDirect

Construction and Building Materials

journal homepage: www.elsevier.com/locate/conbuildmat

Evaluation of resonance acoustic mixing technology using ultra high performance concrete

Aileen Vandenberg [a], Kay Wille [b,*]

[a] Civil and Environmental Engineering, University of Connecticut, 261 Glenbrook Road, Unit 3037, Storrs, CT 06269-3037, United States
[b] Department of Civil and Environmental Engineering, University of Connecticut, United States

HIGHLIGHTS

- Mixing UHPC using Resonance Acoustic Mixing (RAM) Technology® was assessed.
- Comparisons of a RAM mixer and a table top paddle mixer were made.
- Workability and flowability properties differed between mixers.
- UHPC mixed with RAM demonstrated an increase in mechanical properties.

ARTICLE INFO

Article history:
Received 13 June 2017
Received in revised form 15 December 2017
Accepted 27 December 2017
Available online 8 January 2018

Keywords:
Ultra-high performance concrete
Resonant acoustic mixing
Concrete mixers
Mechanical properties
Flow properties
Rheology
Cement

ABSTRACT

This study presents an investigation on the mixing efficiency of Resonance Acoustic Mixing (RAM) Technology® using ultra-high performance concrete (UHPC). In the first part, RAM is optimized through acceleration curve profiles, specific mixing energy, and workability spread flow tests. In the second part, RAM is compared with a regular table top paddle mixer with regards to its effects on workability and flow, as well as, compressive and flexural strength properties. For the UHPC used in this study results showed that: 1) RAM was a viable mixing technology for UHPC, and 2) RAM produced samples of reduced rheological properties, but increased mechanical properties compared to a table top paddle mixer.

1. Introduction

Research in cement hydration, pozzolanic reactivity, particle packing density, and cement-polymer interactions has led to the development of ultra-high performance concrete (UHPC) [1]. UHPC is generally defined as a concrete composite with a compressive strength exceeding 150 MPa (22 ksi), a low water-to-binder ratio (w/b ≈ 0.2) and a high volume (30–50%) of filler and reactive micro-sized particles, such as cement, fly ash, quartz powder and silica fume [2]. Producing high quality UHPC is dependent on an efficient mixing procedure and the type of mixer used. Inadequate mixing may lead to undesirable macroscopic effects on the fresh and hardened state properties of the material [3]. However, a well-mixed mixture permits the concrete constituents to distribute uniformly in its system such that the cementitious materials can hydrate uniformly to create a hardened concrete homogeneous microstructure for better performance [4]. Intensive high-shear mixers have become the industry standard in producing well-mixed UHPC. It has been shown that they are reliable and efficient mixers that reduce mixing times, improve mixing energy distributions, and possess built-in power consumption monitoring [5–9].

Conversely, as the interest grows to produce UHPC as a multi-functional material, such as with the incorporation of carbon nano-tubes [10] or other types of nano-size particles [11–13], or in a more economical manner, such as the utilization of local materials, higher cement replacement, or poorer quality materials [14,15], the mixing efficiency becomes the essence of producing high quality UHPC. This will require more research into not only the mixing procedure, but also the type of mixer used, and hence better understanding of current mixing technologies.

To illustrate, the powder industry employs multiple mixing technologies such as tumbler mixers, gravity silo mixers,

* Corresponding author.
E-mail addresses: aileen.vandenberg@uconn.edu (A. Vandenberg), kay.wille@uconn.edu (K. Wille).

https://doi.org/10.1016/j.conbuildmat.2017.12.217
0950-0618/

pneumatic blenders, and agitation mixers [16]. Notwithstanding, the cement and concrete industry mainly relies on impeller agitation mixers where the main mixing mechanisms are shear and convection [17] via a blade or paddle tool. The reader is referred to [8,18] for a more in-depth review of current concrete mixing technologies.

Concerning cement and concrete, very little research exists utilizing other types of mixers [19–22] used a paint shaker mixer to mix cement paste and assess cement properties such as porosity, chemical shrinkage, and silica/limestone powder activation sites [23] employed power ultrasound-assisted mixing for concrete production and assessed spread and compressive strength properties. They found that the compressive strength increased, while the spread decreased depending on the strength of the ultrasound mixing. Nonetheless, to the authors' knowledge mixing cementitious materials with mixing technologies such as reciprocating movement agitator mixers or bubble acoustic streaming mixers have not been used. Reciprocating agitator mixers work by moving the mixing medium back and forth usually by a vibrating plate to obtain a uniform mixing distribution (Fig. 1a). The power consumed by the mixing is dependent on the frequency, amplitude, and diameter of the plate [24]. Bubble acoustic streaming mixers exploit the acoustic frequency resonance of air bubbles to create micro-mixing convection streaming zones around the mixing media particles (Fig. 1b) [25].

The focus of this research is to mix UHPC by employing a novel type of mixing technology that combines the principles of reciprocating movement agitation and acoustic streaming micro-mixing zones called Resonant Acoustic® Mixing (RAM) technology. RAM is an innovative type of mixing technology that works on vertical reciprocating movement of springs to apply a short amplitude and high frequency (~60 Hz) acoustic pressure wave that induces mixing [26]. Micro-mixing zones and bulk movements of the material are created without the contact of any mixing elements [27]. As an in-container reciprocating movement agitator, RAM has already shown potential in the pharmaceutical [28] and food [29] industries, and thus, could have potential in the cement and concrete industry as well.

In this study, the authors monitored the mixing efficiency of RAM for producing high quality UHPC through acceleration consumption curves, specific mixing energy, and spread flow properties. Then, a designated UPHC mix was selected to assess its fresh state properties and mechanical properties compared to a table top paddle mixer. The aim of this paper is twofold – 1) to test the suitability of RAM for mixing UHPC, and 2) to investigate how RAM mixing compares to a commonly used mixer in the cement and concrete industry.

2. Materials and mixing methods

2.1. Properties of materials

Type I white cement conforming to ASTM C150 [30] was used in all the mixtures. A commercially available high-range water reducer conforming to ASTM C494 [31] Type A & F polycarboxylate (PCE) superplasticizer (SP), with specific gravity of 1.06 and solid content of 29%, was used at 1% by weight of cement (bwoc). White silica fume (SF) and quartz powder (QP) were used as secondary cementitious and filler materials, respectively. Aggregates consisted of fine grade quartz sand (QS) with a medium particle size of d_{50} ~0.18 mm and a maximum size of d_{max} ~0.30 mm. Table 1 provides the mineral and physical composition of the materials used in this study.

2.2. Mix compositions

The mixing proportions were based off the recommendations provided in [2] and are presented in Table 2. The powder proportions remained the same, while the water-to-cement (w/c) ratio was varied between 0.25 and 0.21. The U21 series was utilized for the comparative study with the table top mixer.

2.3. RAM overview

The principal behind Resonant Acoustic Mixing (RAM) (Butte, MT) is illustrated in Fig. 2. The mixing system consists of a three-mass system, spring assembly, and loaded mixing vessel. A motor that subjects the mixing media to a reciprocating agitation movement controls the spring assembly. The system attains resonance when the stored forces in the spring and the inertia forces from the mass equal each other. The resonance of the mechanical

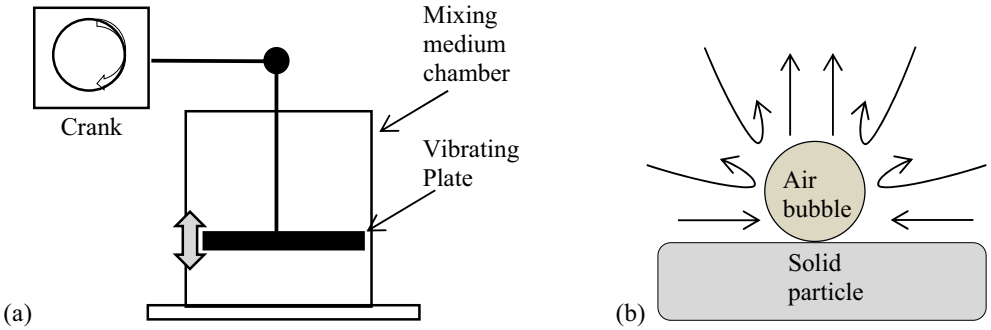

Fig. 1. Two examples of mixing technologies used in other industries: a) reciprocating agitation mixer in which the vibrating plate is moved by a mechanical crank according to [23], and b) acoustic bubble microstreaming in which an air bubble resonates when subjected to a sound field of a matching resonate frequency according to [24].

Table 1
Physical and mineralogical properties of UHPC constituents.

Constituent	Nomenclature	C_3S	C_2S	$C_3S + C_2S$	C_3A	C_4AF	SiO_2	Specific Surface Area/ Mean Particle size
White Cement Type I	C	74%	13%	87%	5%	1%		395 m^2/kg
White Silica Fume	SF						>96%	d_{50} ~0.15 μm
White Quartz Powder	QP						>99%	d_{50} ~1.7 μm
Quartz Sand, fine	QS1							d_{50} ~0.18 mm

Table 2
UHPC mixture proportions by weight.

UHPC Mix Series	Mixer Type	C	SF	QP	QS1	Water	HRWR (% of solid)
U21	R, H	1	0.25	0.25	1.01	0.21	0.01
U23	R, H	1	0.25	0.25	1.01	0.23	0.01
U25	R, H	1	0.25	0.25	1.01	0.25	0.01

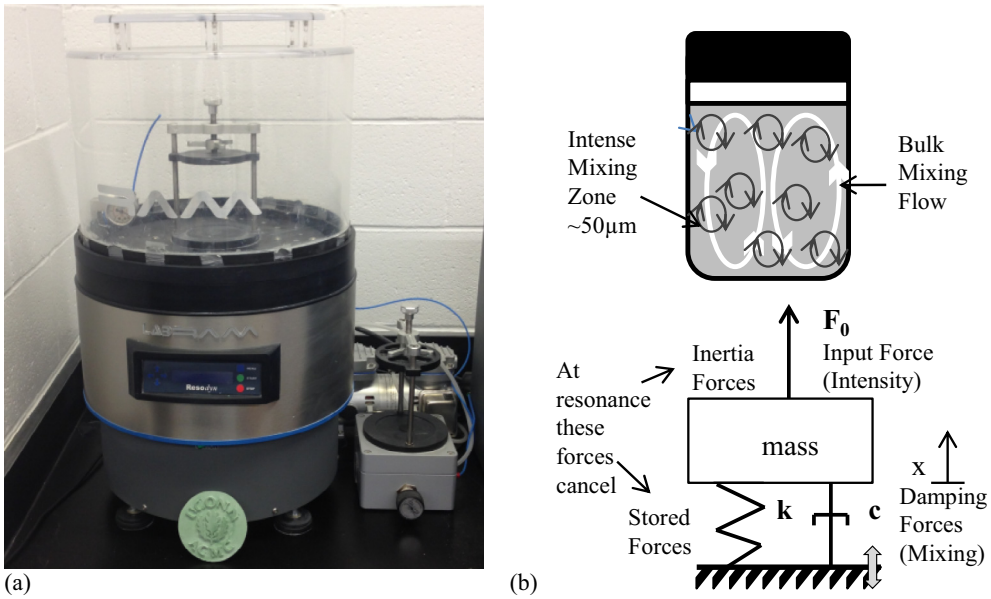

(a) (b)

Fig. 2. a) The acoustic laboratory size mixer LabRAM and b) the schematic of its mixing technology [32].

system translates to the mixing media as a longitudinal acoustic pressure wave with a short amplitude and high frequency. The amplitude is approximately 1.27 cm (0.5 in.) or less for an acceleration of 100G, where G is the acceleration of gravity (9.81 m/s) [29]. The exact frequency is affected by the vessel mass, fill level, compressibility of the material, coupling of the material to the vessel walls, material density, vessel geometry, internal vessel pressure, and mixing regime. RAM adjusts its resonance frequency to account for changes in these factors. For this study, the standard deviation from the nominal 60 Hz resonance was approximately 2 Hz.

A lab scale version of RAM called the LabRAM (R or RM) was used as the mixing source for this research. The LabRAM, capable of accelerating the designated media up to 100G, was controlled through provided OEM software called *RAMWare*. The frequency input parameter was set to *auto* to ensure the mechanical system stayed in resonance, the vital principle behind RAM. By keeping the mechanical system in resonance, the force, and hence the acceleration, can be controlled by adjusting the intensity of the amplitude of the wave (given as '% mixing intensity').

For the fundamental spring-mass-damper system (see Fig. 2b) [33], the equation of motion is given as

$$m\frac{d^2}{dt^2}x(t) + c\frac{d}{dt}x(t) + kx(t) = F_0\sin(\omega_f t) \tag{1}$$

where the left-hand side represents the system forces in terms of inertia forces, with m the mass of the vessel, the mixing forces, with c defined as the damping coefficient, and the stored forces, where k is the spring constant; and the right-hand side is the input force, F_0, and ω_f is the resonance frequency. Eq. (1) represents a forced, damped mechanical vibration system. At resonance, the inertia forces cancel the stored forces resulting in a first order differential equation equal to

$$c\frac{d}{dt}x(t) = F_0\sin(\omega_f t) \tag{2}$$

Solving Eq. (2) for the displacement and subsequently the acceleration results in the following

$$x(t) = A\cos(\omega_f t) \tag{3}$$

$$\ddot{x}(t) = -\omega_f^2 A\cos(\omega_f t) \tag{4}$$

where A represents the peak amplitude to the driving force with respect to the starting center point. It is directly related to the driving force, but inversely related to the damping coefficient. Eq. (4) demonstrates that the acceleration is linearly related to the amplitude. Thus, if the mechanical system is in resonance the '% mixing intensity' directly relates to the acceleration of the material. This means, for example, an input of 70% mixing intensity results in an acceleration of 70G.

The power at peak acceleration was developed by [34] and is given as

$$P_{mix} = \emptyset_{peak}F_{rms}\left(\frac{\Delta P}{100}\right)\frac{a_{peak}\cdot G}{2\pi f} \tag{5}$$

where t_{mix} is the total mixing time and P_{mix} is the total power that goes into the mixture, $\emptyset_{peak}$ is the correction factor from peak to root-mean-square (rms), F_{rms} is the machine force constant, P is the difference in power intensity from loaded to unloaded mass, a_{peak} is the peak acceleration, f is the resonant frequency, and G is the gravitational constant. The correction factor and machine force are machine variables and are set to a value of 0.707 and 70 ± 4 N,

respectively. Hence, using Eq (5) the total specific mixing energy can be calculated as

$$E_{mix} = \frac{P_{mix} \cdot t_{mix}}{mass} \quad (6)$$

2.4. Sample preparation

RAM samples were prepared using the input routine given in Fig. 3a using the following 4-step mixing protocol (Fig. 5a):

1. Mix the dry materials all together at an intensity of 95% for 120 s. [2] notes that by mixing all the dry constituents first the chance that agglomerates of very fine particles will form is reduced. Though, contrary to [2], the authors found that the order of placement in the mixing vessel did not make much of a difference; however, to ensure good compaction of the less dense materials (e.g. silica fume), aggregates were added last;
2. After dry mixing, the routine was paused and a well was formed in the dry mix. The water was combined with the HRWR before being poured inside the well. The well was subsequently covered up before returning the vessel to the LabRAM;
3. The mixture mixed for 50–215 s after water contact before pausing for 30–90 s to allow the heat to dissipate and to scrape an excess material off the sides of the vessel;
4. Finally, the mixture was subjected to an additional 60–210 s of mixing. The response to the intensity routine (e.g. the acceleration) was then recorded (Fig. 3b).

Samples were also prepared using a three-speed Hobart laboratory paddle bench mixer (H or HM) with a standard designated paddle (Fig. 4).

The mixing protocol (Fig. 5b) followed the recommended protocol given in [2]. It consisted of the following 4 steps:

1. The silica fume and sand are mixed together for 3 min at speed 1 (107 rpm);
2. The quartz powder and cement are added for another 3 min of mixing at speed 1;
3. The water is combined with all the HRWR and poured into the powders for 2 min;
4. The speed is increased to level 2 (198 rpm) for another 11–15 min.

Total time of mixing from dry to wet was between 19 and 25 min. For this study, the fill level of the mixing container was around 1.5–2.0 L or about 17% fill level.

3. Experimental program

3.1. RAM monitoring methods

The practice of monitoring the mixing evolution of a concrete's microstructure through the power curve, or the cohesion curve, has become the most developed monitoring technique in the last decade [5,8,35,36]. From Eq. (5) the power is linearly related to the acceleration. Therefore, the acceleration curves were used to monitor the UHPC microstructure development for this study. Moreover, the stages of mixing were based on [37,38] after liquid loading, where the acceleration curve is divided into five stages of mixing that are each defined by force dissipation mechanisms (Fig. 6). The fluctuation of the acceleration curve is defined as the difference between three consecutive measurements.

In the first stage, immediately after the liquid is introduced into the mix, the acceleration sharply increases as the microstructure is in a dry granular state dominated by frictional forces. After about 10–15 s of mixing there is a slight change in curvature of the acceleration curve, corresponding to a decrease in the fluctuation curve; this is the start of the second stage. During this stage the microstructure develops into a wet granular structure that is dominated by frictional and cohesive forces as now the water is slowly saturating the granules and forming bridges with surrounding granular structures. The leveling of the acceleration curve corresponds to the saturating of the granules and the slight dip before the maximum peak acceleration, a_{peak}, corresponds to the saturation of the liquid bridges between granules. This peak is defined as the maximum cohesion point and the end of the second stage. For the third stage the acceleration curve decreases, and the microstructure resembles a hard paste dominated by cohesive forces.

The fourth stage is defined by the second transition point, the fluidity point. Here the acceleration curve starts to increase again with a fluctuating response. The microstructure is now a soft granular fluid suspension dominated by cohesive and viscous forces. The fluctuations are due to granules slowly breaking up and dispersing into the suspension. The fifth and final stage is defined when the acceleration and fluctuation curves level off. The microstructure has become a fluid suspension dominated by viscous forces.

As with an intensive shear mixer, the time, the power, the water-to-cement ratio, and the fill level all have an influence on the acceleration curve and change the location of the cohesion and fluidity points [35]. Hence, a series of tests (Table 3) were performed to monitor how the acceleration and fluctuation curves change as these four parameters change for RAM mixing.

These tests were then analyzed to find the most optimized routine for each specific UHPC tested in this study using specific

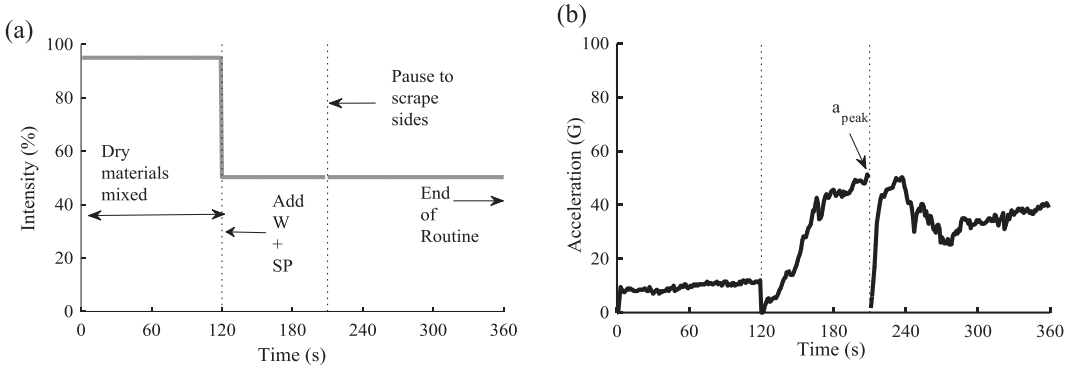

Fig. 3. An example of the a) input intensity routine and b) the acceleration response measurement. The maximum acceleration is taken as a_{peak}.

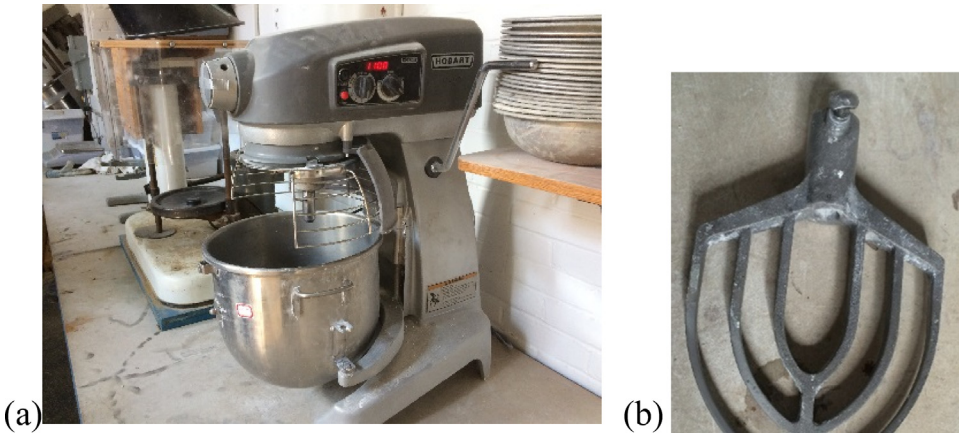

Fig. 4. a) The Hobart 3-speed 12-L capacity paddle mixer and b) its associated paddle.

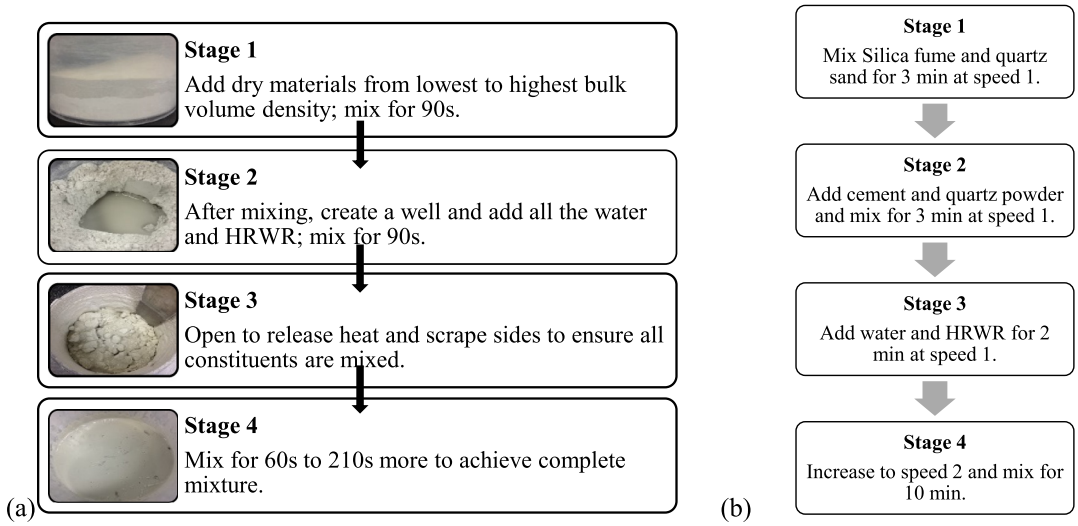

Fig. 5. The 4-stage mixing protocols for a) the resonance acoustic mixer and b) the table top paddle mixer.

mixing energy and spread flow workability tests. An average of 3 measurements per sample test were taken. The standard deviation was taken to be twice the median of the measurements.

3.2. Workability

The allowable mass limit for the LabRAM is 500 g and the volumetric limit of the mixing vessel used is 500 mL. Due to the low bulk density of the non-compacted dry powders filling the mixing vessel to its maximum capacity of 500 mL, about half this volume of fresh cementitious material can be produced. This amount of material is not enough to fill the standard cone (1.376 mL) described in ASTM C230 [19]. Hence, a modified cone (Mini) was manufactured with dimensions half of the standard cone (Standard), and thus a volume ratio of 1:8, to test the spread flow properties (Fig. 7a). The volume to fill the mini cone is 172 mL.

All UHPC mixes were tested using both cones. The corresponding spread diameter ratios between the two cones were then recorded using standard measuring tape of an accuracy of a millimeter and averaged over 4 measurements (Fig. 7b). Spreads were taken 20 min after water contact with the cement. Comparisons of the spread flow values of the standard cone to the mini cone showed a nearly constant spread ratio of 2.5 (Fig. 8) with an R square value of 0.984.

3.3. Steady state rheology

Steady-state flow rheological measurements were obtained using a Malvern Kinexus Pro+Rheometer (Fig. 9a) with a cup and serrated bob geometry (Fig. 9b). Rheological tests were conducted between 15 and 20 min after water contact with the cement to ensure the material was in the dormant period [39]. The steady-state protocol utilized a hysteresis loop sequence as used in previous studies for normal concrete [40,41]. The protocol was as follows (Fig. 9c):

1. Pre-shear at a constant shear rate of 10 s^{-1} for 30 s,
2. Rest for 30 s,
3. Increasing linear shear ramp from 0.9 s^{-1} to 10 s^{-1} for 90 s,
4. Decreasing linear shear ramp from 10 s^{-1} to 0.9 s^{-1} for 90 s.

The area within the hysteresis loop was computed to relate to the structuration of the material [42] as shown in Fig. 10.

As with most concretes that contain high ratios of polymer, a standard Bingham flow model (Fig. 11a) results in negative yield stress values due to the non-linear behavior of the material [43]. Therefore, a modified Bingham model (Fig. 11b), given in Eq. (7), was applied to the rheological data.

$$\tau = \tau_0 + \mu\dot{\gamma} + c\dot{\gamma}^2 \quad (7)$$

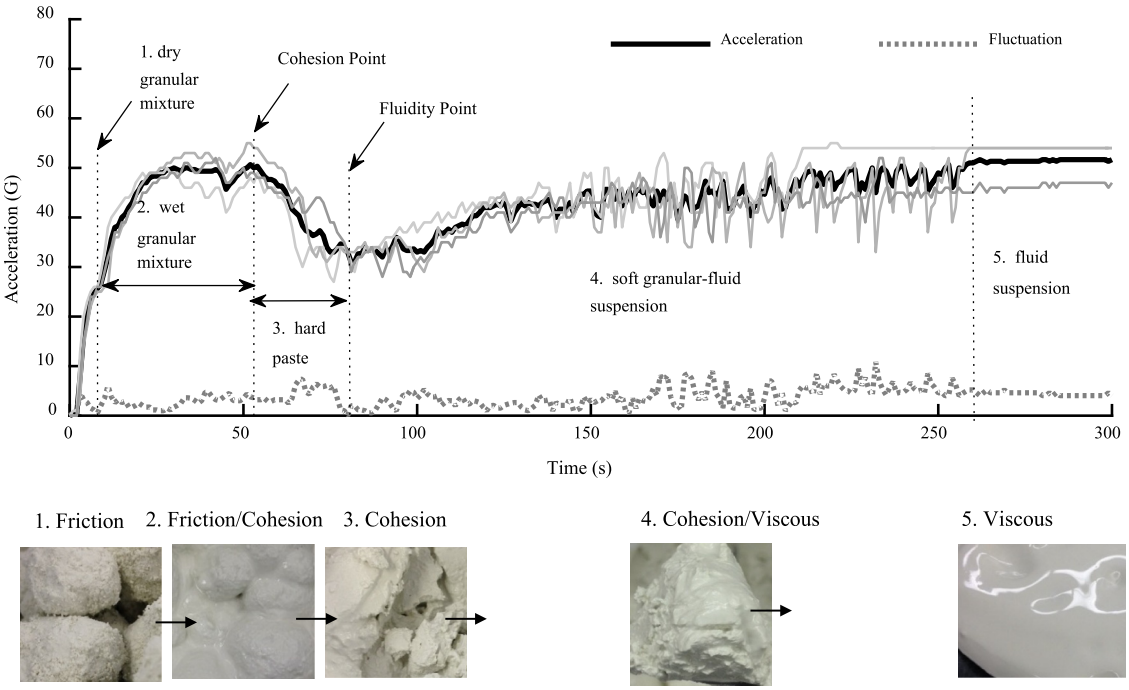

Fig. 6. A mixing acceleration measurement profile with its fluctuations between 3 different measurements. Each mixing stage and transition point is identified and associated with its respective dissipation origin forces.

Table 3
Mixing parameters of RAM monitored.

Series	Intensity (%)	Fill Level (%/g)	Water-to-Cement	Mix Time (s)
Intensity	40, 50, 60, 70, 80	44/221	0.25	300
Fill Level	50	50/250, 70/350, 100/500	0.23	300
W/C	50, 70	50/250, 100/500	0.21, 0.23, 0.25	300
Time	70	100/500	0.25	150, 270, 300

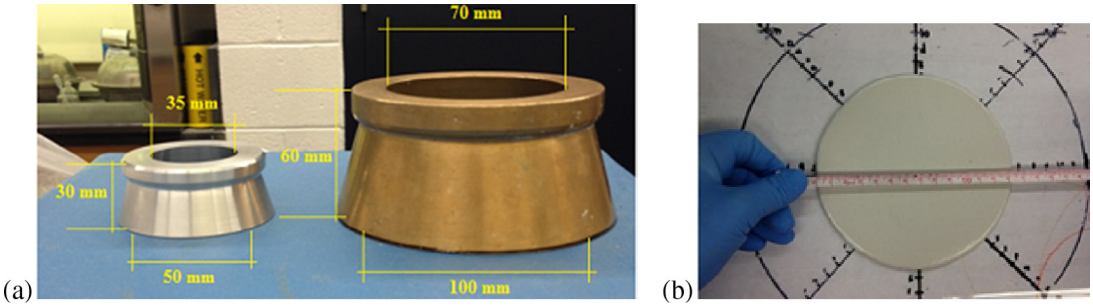

Fig. 7. a) Spread Flow measurements were taken using a mini cone with half the dimensions of the cone designated in ASTM C230, and b) measured using a tape measure.

This model is preferred over the Herschel-Bulkley model (Fig. 11c) because its parameters can be related to the physical properties of yield stress and plastic viscosity. In Eq. (7) the yield stress, defined as the stoppage of flow or when the shear stress in the material is no longer plastic, is given by τ_0, the plastic viscosity, defined as the resistance to flow, is given by μ, and the second order term, c (Pa-s^2), relates to the shearing behavior of the material. If shear stress decreases with an increase in strain ($c/\mu < 0$) the material is said to be shear thinning. Conversely, if shear stress increases with an increase in strain ($c/\mu > 0$) the material is designated as shear thickening. If the shear stress is linear with strain ($c/\mu = 0$), then it is Newtonian.

3.4. Mechanical properties

ASTM C109-Standard Test Method for Compressive Strength of Hydraulic Cement Mortars (Using 2-in. or [50-mm] Cube Specimens) [44] was followed for compression testing. Specimens were cast in 50-mm (2 in.) cubic brass molds and vibrated for approximately 30 s. The specimens were covered and placed in a controlled curing room for 24 h at 20 °C before being demolded and placed in a lime-saturated water bath at 20 °C. Before testing, the load surfaces were ground to ensure the specimens were loaded uniformly leading to results with high consistency. Specimens were tested at 3 days, 7 days, 28 days, and 56 days.

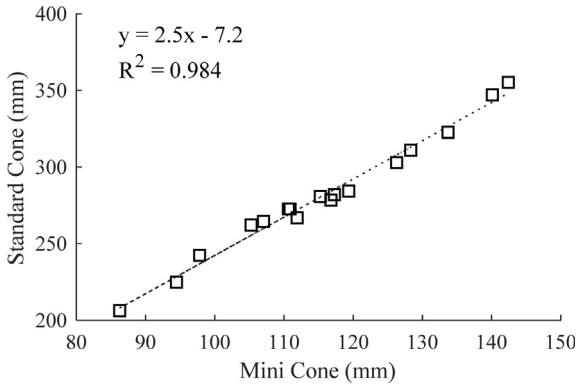

Fig. 8. Correlation between the ASTM standard and the modified mini cone.

The compressive strength was taken as maximum force divided by the average area of the load face surfaces.

A non-standard three-point bending test was used to obtain the maximum flexural strength. Beams with average dimensions of 15 cm × 2.5 cm × 2.5 cm (6 in. × 1 in. × 1 in.) were cast in a high-density polypropylene (HDPE) beam mold. The specimens were covered and placed in a controlled curing room for 24 h at 20 °C before being demolded and placed in a lime-saturated water bath at 20 °C. Specimens were then tested at 7 days and 28 days. Averages were taken for 3 specimens per mix with the standard deviation taken per sample.

4. Results

4.1. Monitoring RAM through acceleration curves

Acceleration and fluctuation curves for mixing intensities 40%, 60%, and 80% are shown in Fig. 12a–c and for 50% in Fig. 14a. [45] defined two types of granular growing behavior for wet powder agglomeration, that is, Stepwise Growing Behavior (SGB) and Continuous Grown Behavior (CGB). From these results it can be observed the lower % mixing intensity levels are of a SGB nature, while the curve for 80% mixing intensity is more of a CGB form. The difference between the two is whether the material acts as individual agglomerates or as one large agglomerate. In a vertical oscillating system, at maximum amplitude the particle can experience free fall if there are no other forces acting on it. It is assumed that this is the case for RAM. Thus, the maximum amplitude, A, velocity, v, and height, h, a particle can achieve through free fall is given as

$$A = \ddot{x}/\omega_f^2 \tag{8a}$$

$$v = A\omega_f \tag{8b}$$

$$h = v^2/2G \tag{8c}$$

where $\ddot{x}$ is the maximum acceleration, ω_f is the resonance frequency, and G the gravitational constant. Increasing the intensity increases the acceleration and thus the free fall height the material experiences with the vertical oscillatory movement. According to Eq. (4) when the RAM mixer is in resonance the peak acceleration increases linearly with intensity. Hence, for a mixing intensity of 40%, the material experiences 40G of acceleration. For a resonance frequency of 60 Hz, this equates to an amplitude of 2.76 mm, a velocity of 1.0 m/s and free fall height of 55 mm. For an intensity of 80%, the amplitude and velocity are twice this, but the free fall height is 4 times greater.

It can also be seen from the fluctuation curves that the start of the largest fluctuation peak correlates to the cohesion point of the mix and the end correlates to the fluidity point (Fig. 12a). This type of behavior has been seen in other studies as well for power fluctuation curves [35,38]. Furthermore, when the fluctuation curve becomes constant or very close to zero, this is denoted as the time to reach a state of full dispersion. The time to reach this point decreases with an increase in mixing intensity. Past research has denoted a similar point called the stabilization time [5,8] which can be related to the optimal mixing time. Finally, it can also be observed that the acceleration curve, once it reaches this point becomes the same value as the mixing intensity, e.g. 80G at 80% mixing intensity, and therefore, indicating the RAM is at complete resonance once it reaches full dispersion.

Fig. 13 shows the acceleration and fluctuation curves for the Fill Level Series. Fill level herein is defined as a percentage of mass, with 100% or 500 g being the maximum fill level. Results show that at a 50% (250 g) fill level, the peak acceleration is 5–10% higher in intensity than the mixing intensity level, while the 70% (350 g) fill level is 5% lower. For 100% (500 g) fill level, the peak acceleration is reduced by approximately 10–15%. As the amplitude is inversely related to the damping coefficient by the relationship F_0/c (see Eq. (2)), then likewise the acceleration is too. At resonance, the system is critically damped, and c is equal to $2\sqrt{km}$ [46]. Hence, if there is a 50% increase in mass, there must be about 14.1% reduction in acceleration, which is what is presented in Fig. 13c for the average acceleration curve. Furthermore, as the fill level increases the time it takes to reach the cohesion and fluidity points also increases. The reduction in acceleration means a reduction in

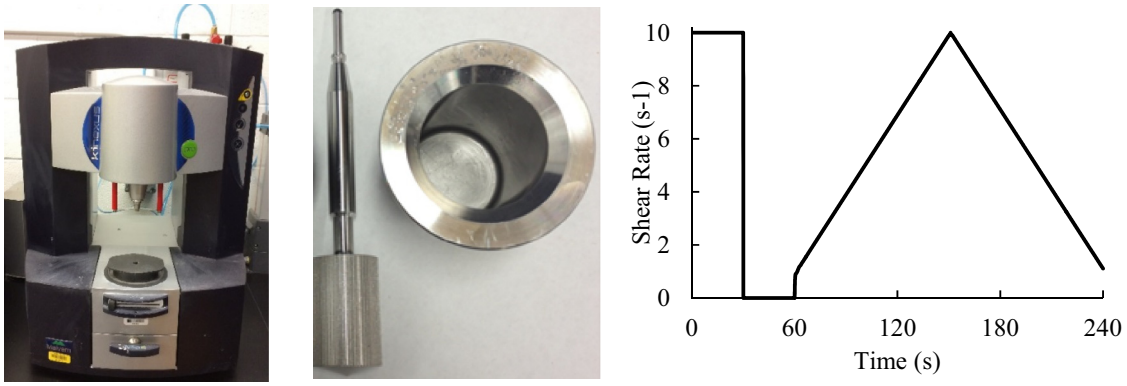

(a) Malvern Kinexus Pro+. (b) Cup and bob geometry. (c) Steady-State rheological sequence.

Fig. 9. Flow rheology testing a) equipment, b) geometry, and c) protocol used in this study.

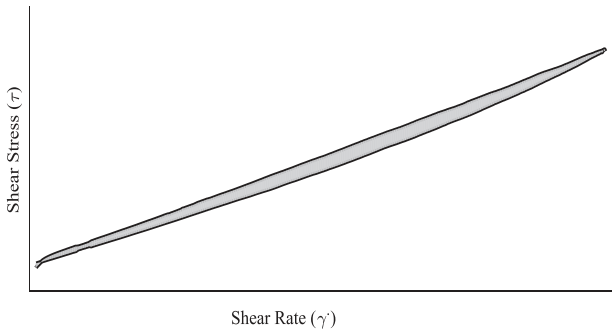

Fig. 10. Typical thixotropic hysteresis loop in this study. The grey area is related to the energy needed to breakdown the material's structure.

mixing force intensity, and hence, a difference in cohesion behavior of the mixture is observed.

As the apparent volume of the mixing level is initially full at the start of mixing, there is less space to fully reach the maximum free fall height adding to the reduction in impact force the material feels from the vessel's boundaries. Nonetheless, like the Intensity Series results, the width of the largest fluctuation peak, or the largest two consecutive peaks, corresponds to the stage of mixing between the cohesion and fluidity points, and the point where the fluctuation curve reaches a constant state denotes the final state of the mixture. From Fig. 13b and Fig. 13c it appears more time was needed for higher fill levels to reach this point.

In Fig. 14 the results for the W/C Series are presented. Fig. 14a–c show results for a fill level of 50% and mixing intensity of 50%, while Fig. 14d–f show results for a fill level of 100% and mixing intensity of 70%. Several observations can be made. First, the length of the cohesion stage increases with decreasing w/c ratios. This is expected as it has been seen in past research [5,8,35] with decreasing water to powder ratios. Second, for the 50% fill level results, the peak acceleration increases as the w/c ratio decreases going from the expected 50% mixing intensity for w/c 0.25 (Fig. 14a), to an increase of 5% to 10% for w/c 0.23 (Fig. 14b) and 0.21 (Fig. 14c), respectively. This type of behavior is not intuitive as the opposite is expected. Yet, recalling Fig. 12c for 80% mixing intensity, where the length of the cohesion stage increased with an increase in intensity being attributed to the switch between SGB to CGB, then it is suggested that when the w/c ratio decreases the material accelerates not as individual agglomerates, but as one large agglomerate. Thus, the RAM machine needs to increase the acceleration to break the cohesive bonds between the material and the vessel walls before further liquid distribution can take place. Conversely, for the 100% fill level, the peak acceleration decreases with decreasing w/c ratios. It is 20% less than the % mixing intensity for the higher w/c ratios of 0.25 and 0.23 and close to 30% less than the mixing intensity for the lowest w/c ratio. Lastly, the length of the cohesion stage for the highest w/c ratio (14 d) remains the same (compared to Fig. 14a), but for lower w/c ratios the length decreases, indicating the increase in fill level is helping the cohesion of the material along.

4.2. Monitoring RAM through specific mixing energy and spread flow

Shown in Fig. 15 are the specific mixing energies and spread flows for the specified test series given in Table 3. The specific mixing energy (SME) of a mix is a property that is used to compare laboratory mixes to field mixes for oil well cement slurries [47,48]. It is dependent on the time of mixing and the total mass of the system (see Eq. (8)).

In Fig. 15a the spread-flow shows a decreasing trend as the % mixing intensity increases from 50% to 80%, while the SME shows an inverse trend. For the Intensity series, the time of mixing was the same for each intensity, however, the acceleration curves in Fig. 12 demonstrate that the optimal mixing time varied for each intensity level. For example, for 80% mixing intensity the optimal mixing time was on average 200 s. Using this in Eq. (8) results in an optimal SME closer to 85 kJ/kg, which is the SME value for 70% mixing intensity. Nonetheless, even this value is not the most optimum SME value, which for this mix series is around 45 kJ/kg for 50% mixing intensity.

For the Fill Level mix series, the spread flow values are larger at 50% fill level, but level out by 70% fill level (Fig. 15b). With an increase in fill level, the SME decreases and thus a longer time of mixing and/or a higher peak acceleration is needed to obtain the same SME for a lesser fill level. Even still, the spread flow values do not appear to be affected from the drop in SME.

In Fig. 15c and d the change in w/c ratio and its effects on the spread flow and SME values are depicted. The increase in spread flow values is expected when the w/c ratio is increased. However, an increase in spread flow does not always correlate to an increase in SME values as these values change according to mass, mixing time, and % mixing intensity levels. For example, the spread values increase for the U25 mixture when both the fill level and % mixing intensity increase (Fig. 15d), while the converse is true for the U21 mixture (Fig. 15c). The spread flow values also increase when the mixing time increases (Fig. 15e), though it can also decrease if the mixing time is too long (Fig. 15a).

4.3. Comparison of fresh state properties of RAM to a table top paddle mixer

To assess how RAM mixing affects the fresh state and hardened state properties of a given UHPC mixture, a comparative study to a

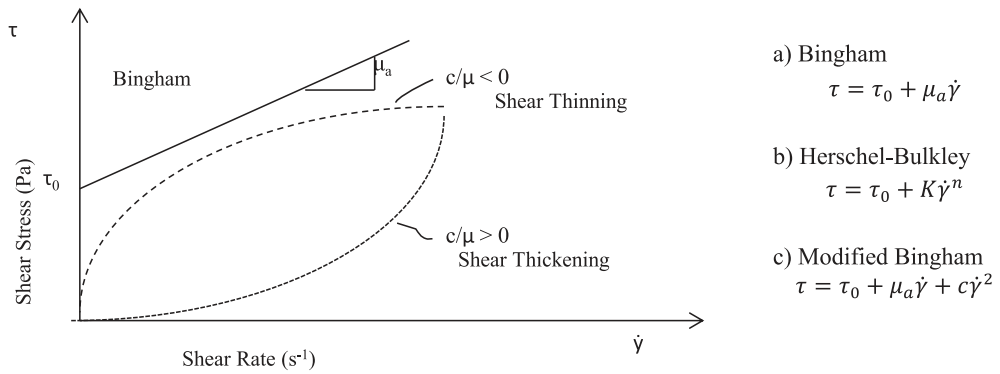

Fig. 11. Different rheological behaviors and the models applicable to UHPC [43]. For this study the best fitting model was the Modified Bingham model.

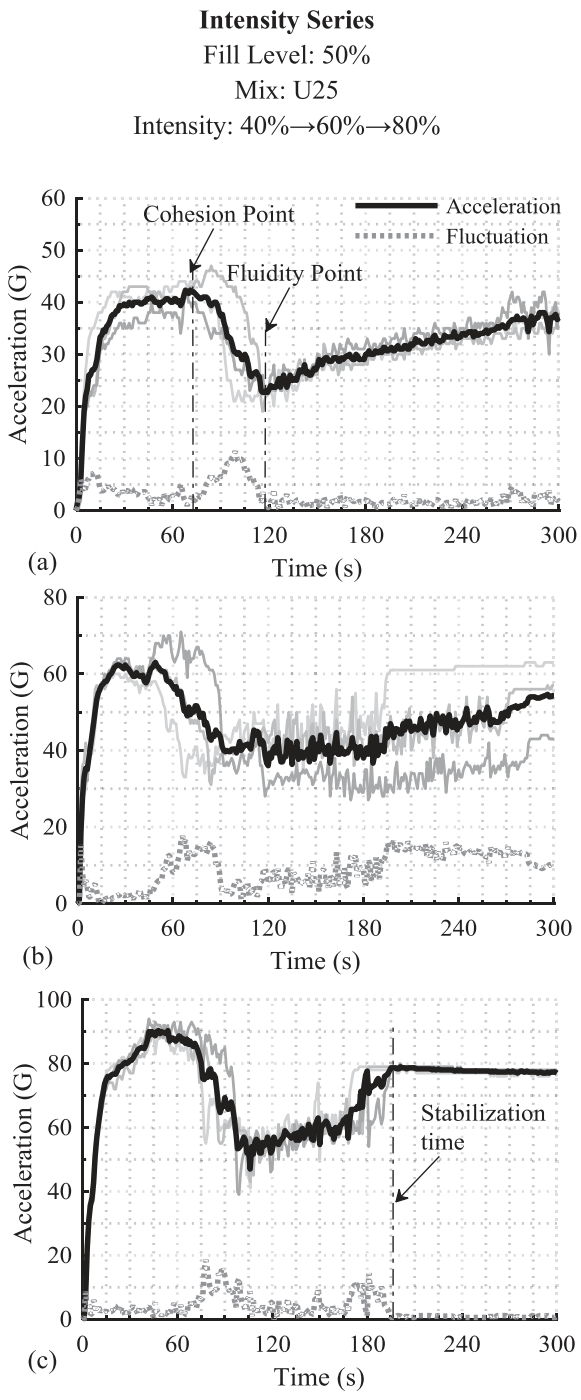

Fig. 12. Average acceleration and fluctuation measurements for the Intensity Series a) 40%, b) 60%, c) 80% with a fill level of 50% for the mix U25 series.

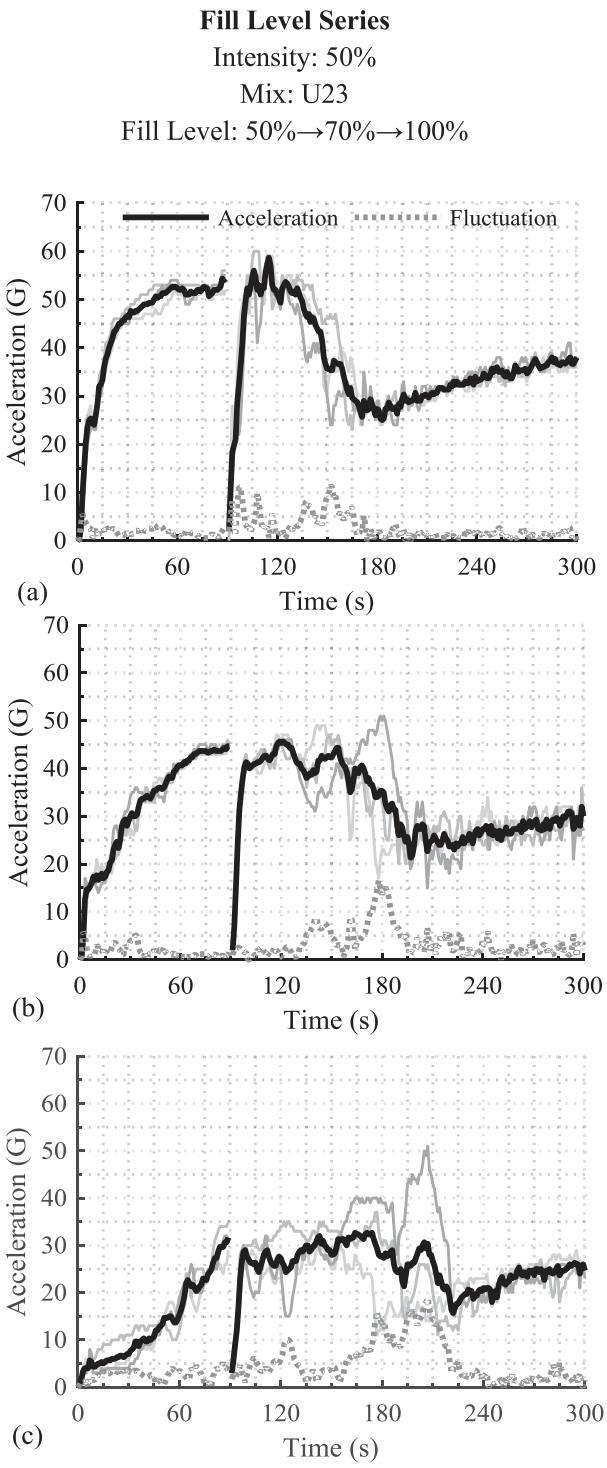

Fig. 13. Average acceleration and fluctuation measurements for the Fill Level Series a) 50% (250 g), b) 70% (350 g), c) 100% (500 g) with an intensity of 50% for the mix U23 series.

table top paddle mixer was undertaken. All results for the RAM were for a mixing intensity of 70% and a fill level of 100% (500 g), as the best spread values for all the UHPC mixtures (see Fig. 15.) were found at this setting. Fig. 16 shows the results of the rheological tests. The area enclosed is the hysteresis area which represents the energy needed to break down a material's structure as well as the amount of structuration that builds up after shearing stops [42,43]. The largest differences can be found for the U25 mixture series and the smallest for the U23 series.

Shown in Fig. 17 and summarized in Table 4 are the fresh state properties from these flow curves and the spread flow cone tests between the two mixers. In Fig. 17a the spread flow values show an increase in spread value for the U21-H and U25-H series (see Table 2), but not much difference between the two mixers for the U23 series. Fig. 17b shows the yield stress values between the two mixers with the U21-R series showing a much higher yield stress than the U21-H series. Such a difference should be reflected in the spread value, however, as the spread flow depends on a variety of other factors than the material itself such as the surface

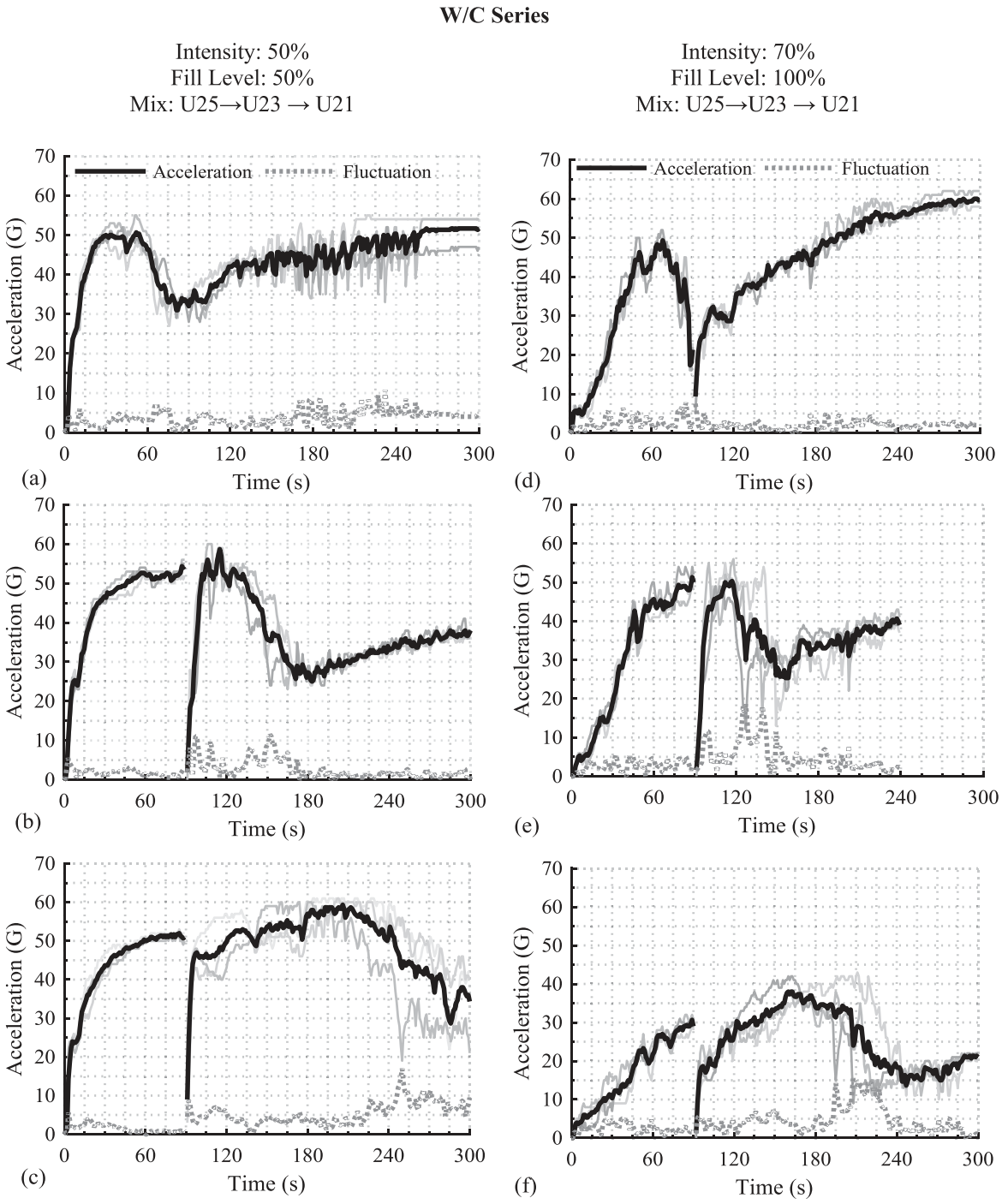

Fig. 14. Average acceleration and fluctuation measurements for the W/C Series. LHS: the fill level and intensity level are each 50%. The mix series are a) U25, b) U23 and c) U21. RHS: the fill level is 100% and the intensity level is 70%. The mix series are d) U25, e) U23 and f) U21.

tension of the spread cone, the spread surface, and the thickness of the spread compared to the diameter, the spread value can only be taken as an approximation of the yield stress. The modified Bingham model estimates closer to the true value of the yield stress [43,49].

In Fig. 17c, the viscosity values for the U23 series are the same, while for the U25 series the RAM mixer has a higher viscosity. The hysteresis loop areas are presented in Fig. 17d. Overall, the RAM mixer shows higher shear thickening behavior (Fig. 16) than the Hobart mixer. This explains why the yield stress is higher and the spread values are lower for the RAM mixer.

4.4. Comparison of mechanical properties of RAM to a table top paddle mixer

Since the U21 series showed more differences in the fresh state properties between the RAM mixer and the Hobart mixer, this series was chosen to conduct mechanical tests for the hardened state properties comparison. Compression results are shown in Fig. 18a and flexural results in Fig. 18b. The first observation that can be made is that there is a considerable increase in mechanical strength comparing the results using the RAM mixer to using the Hobart mixer. The most notable increase is in the early age properties at

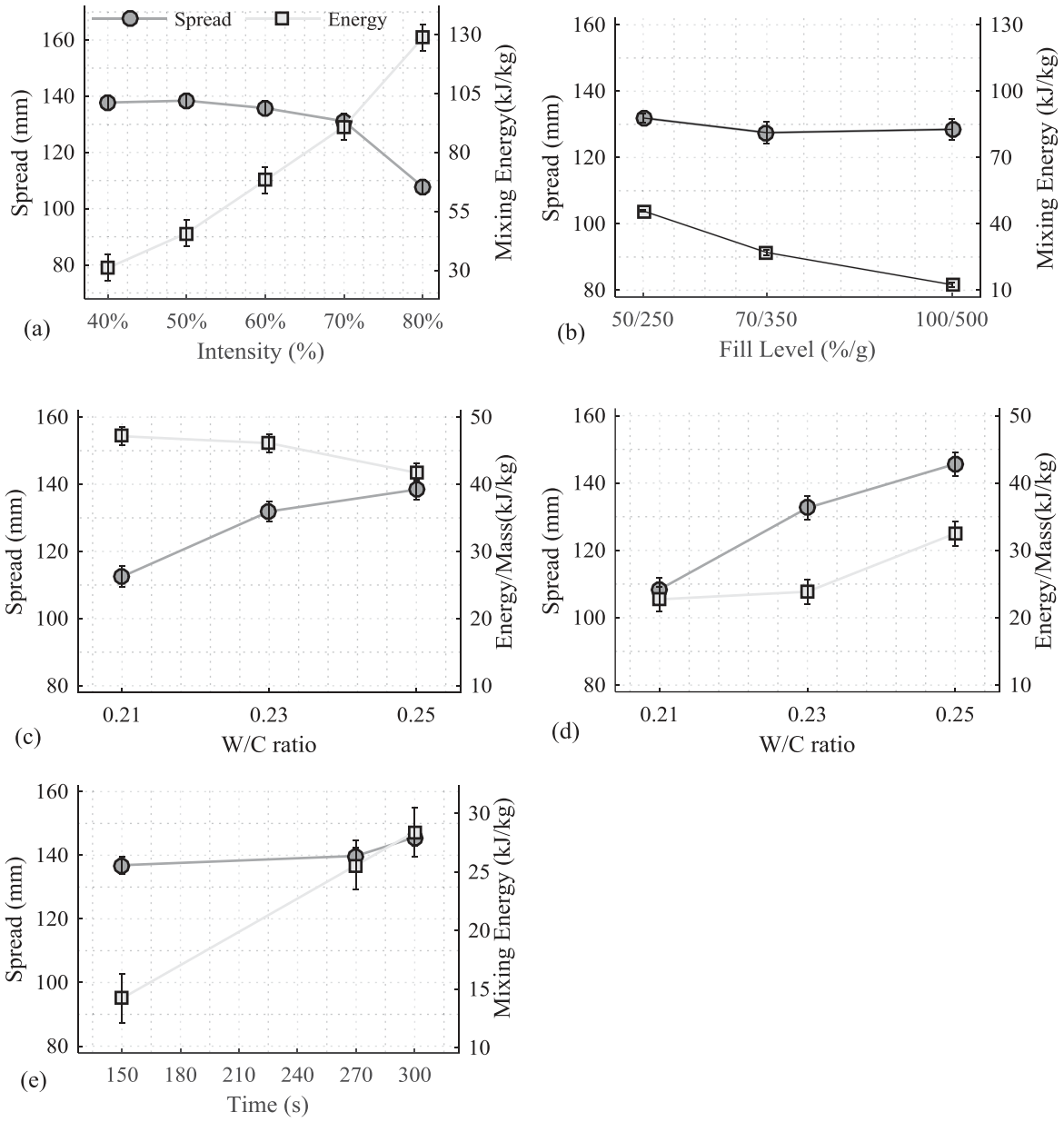

Fig. 15. The spread flow values compared to the specific mixing energy: a) Intensity Series, b) Fill Level Series, c) W/C Series where the fill level and intensity level are each 50%, d) W/C Series where the fill level and intensity level are 100% and 70%, respectively, and e) Time Series for U25 where the fill level and intensity level are 100% and 70%, respectively.

3 days (7 days for flexure) where there is a strength improvement of around 30% while the later age strengths show between 16% and 20% improvements in strength.

The improvement in mechanical strength properties can be attributed to a variety of factors such as reduction in the air content, better dispersion or packing of the particles, or an increase in microstructural development with being affected by the energy imparted to the mixing container. The air content affects the compressive strength as follows [2]

$$f'_c = -216 \times (w/c) \times air^{1/3} + 230; f'_c[\text{prism}]\text{is in MPa} \quad (9)$$

Thus, for example, an air content of 10% reduces the compressive strength by approximately 21 MPa. The difference between the f'_{c-28d} of the U21-H and U21-R mixes is about 28 MPa. This would mean the air content of the U21-H would have to be on the order of 25%. According to [2] the air content of the U21-H mix is between 1 and 5%. Thus, it is inferred that the improvement to the mechanical properties is a result due to better packing of the matrix and/or change of microstructure, such as seen with a high intensive mixer. Therefore, it is of value to verify, at least qualitatively, that the RAM mixer acts like a high intensive mixer.

4.5. Verification if RAM is an intensive mixer

To be a high intensive mixer usually means the mixer imparts a high shearing action to the system. As the RAM does not work on a shearing principle, but instead of a resonant acoustic vibrational principle, it is not apparent whether it can be considered a high intensive shear mixer. All the properties presented in the previous sections illuminate high intensive mixing properties. The acceleration curves and the specific mixing energy show values often seen in high intensive shear mixers. In fact, the American Petroleum

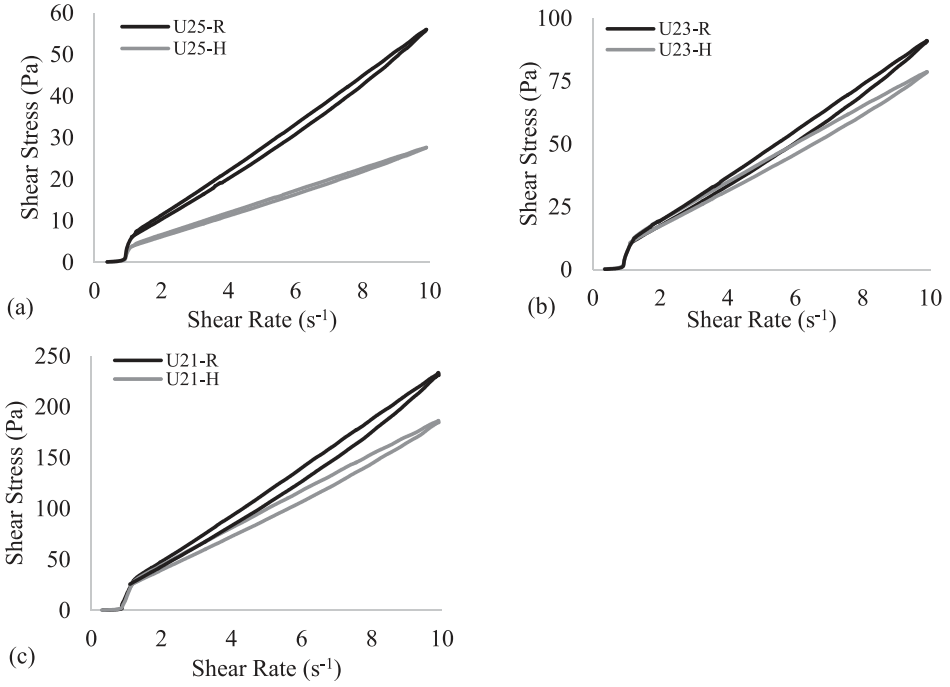

Fig. 16. Average shear flow curves for a) U25, b) U23, and c) U21, where R means RAM mixer and H means Hobart mixer.

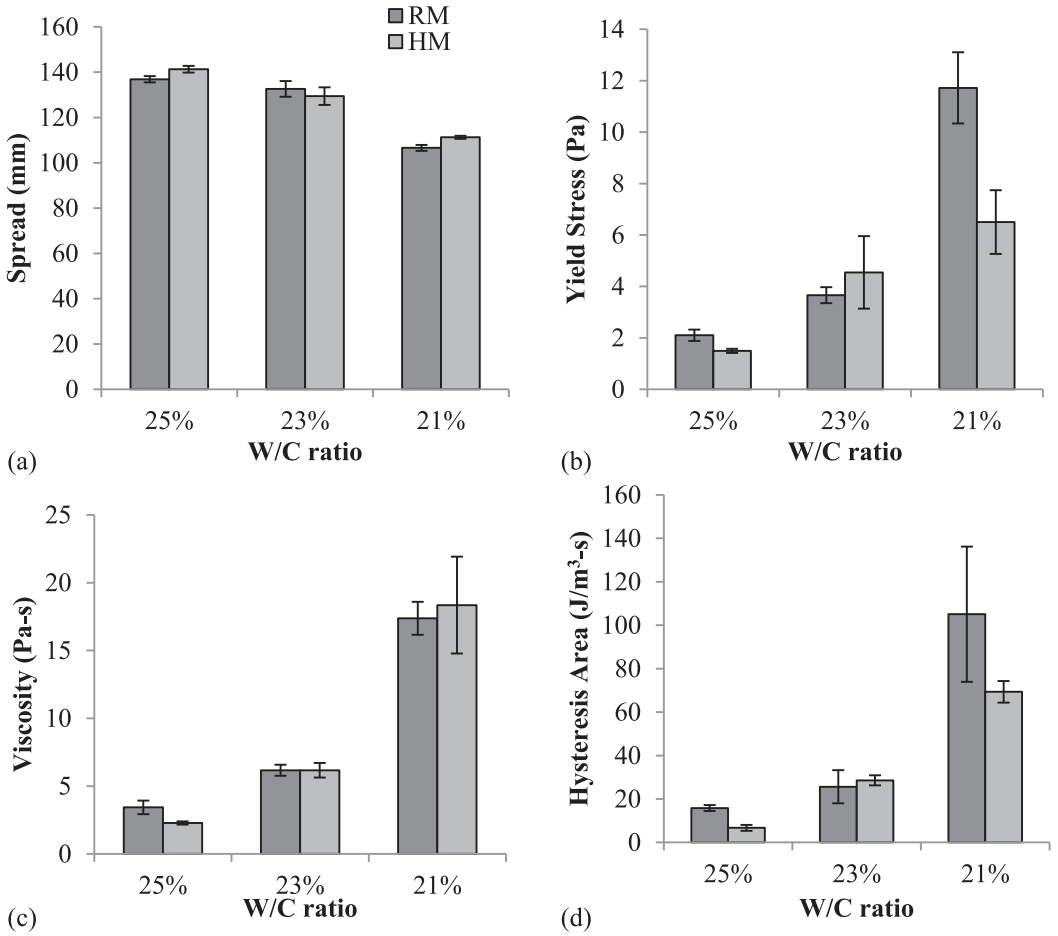

Fig. 17. Flow properties. a) spread-flow, b) modified Bingham yield stress, c) modified Bingham viscosity, and d) hysteresis area.

Table 4
Summary of fresh state rheological properties.

Sample	Hysteresis Loop Area ($J \cdot m^{-3} \cdot s^{-1}$)	τ_0 (Pa)	μ (Pa·s)	c ($Pa \cdot s^2$)	Spread (mm)	$Spread_{eqv}$ (mm)
U25 – R	15.81	1.95	3.93	0.15	136.9	334.4
U25 – H	6.70	1.49	2.28	0.03	141.3	345.4
U23 – R	25.60	3.82	6.40	0.23	132.6	323.7
U23 – H	28.57	4.55	6.17	0.12	129.4	315.7
U21 – R	83.08	9.70	15.43	0.68	106.6	258.8
U21 – H	69.34	6.50	18.35	0.42	111.3	270.4

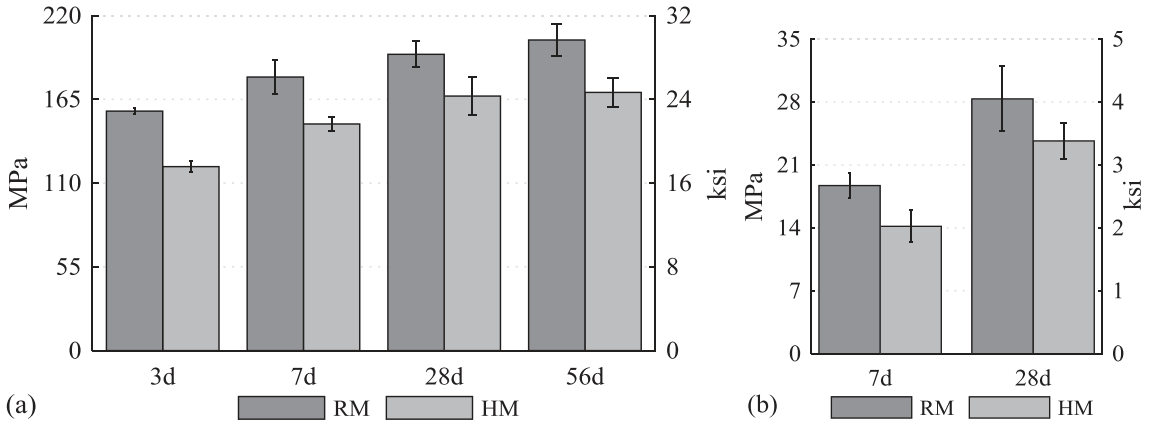

Fig. 18. U21 mix average a) compressive strengths for 3 d, 7 d, 28 d, and 56 d, and b) flexure strengths for 7 d and 28 d. HR.

Institute (API) SME standard for a standard paddle mixer is on the order of 5.5 kJ/kg [47]. The RAM mixer shows SME values one to two orders higher than these energy values. The increase in rheological properties, decrease in workability, and increase in mechanical properties all show behavior of a high intensive shear mixer for UHPC. Thus, to further explore the hypothesis that RAM mixing is high intensive mixing, the acceleration curve profile, converted to normalized power using Eq. (5), of the RAM mixer is compared to the power curve profile of a 6 L Eirich (Hardheim, Germany) high intensive shear mixer (Fig. 19 and Table 5). The fill levels are kept between 80 and 90% and the temperature was also monitored.

The first remark that can be made is that the normalized power curves share the same profile. While the peak energy is different (418 kJ for Eirich and 17 kJ for RAM) the specific mixing energy is close to similar. Where the two mixers deviate is the spread values. The Eirich has a higher spread value than the RAM, signifying that the workability is better. This can partially be attributed to the difference of 4 °C final temperature between the two mixes. Other factors that can affect the workability are the air content and the consistency of the mix. Further study is needed of the RAM to quantitatively verify that it is an intensive mixer, but qualitative evidence demonstrates that is has the potential to be one.

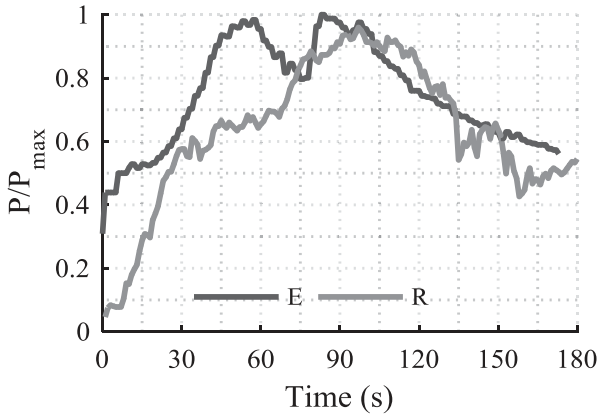

Fig. 19. Normalized power consumption curve comparison of high intensive shear mixer to RAM mixer.

Table 5
Comparison of properties between Eirich and RAM.

	Eirich	RAM
Container Fill Level	80%	90%
Energy (kJ)	418	17
Energy/mass (kJ/kg)	34.9	34.0
Spread (mm)	113	104
Max Temp (°C)	35.0	39.1

5. Discussion

The previous section established that the RAM mixer is qualitatively a high intensive mixer. While, the principle of RAM is not shear mixing, results from intensive shear mixing can still be applied to better understand and discuss the nature of the microstructural development of the UHPC in this study.

RAM works on the principle of transferring the potential energy of its springs to the kinetic energy of the particle collisions inside the vessel. There is no shearing tool interaction with the material and hence it can be said that RAM energy distribution is uniform. It is known that high mixing intensity accelerates the hydration kinetics and changes the physical and chemical nature of cement paste [50–52]. These phenomena originate from the high shear forces increasing the surface diffusion and decreasing the thickness of the diffuse double layer around the cement particles, and thus increasing the interparticle attractive forces [52] . The results are an increase in rheological properties, a decrease in workability, and increase in thixotropy, and sometimes an increase in mechanical strength. Thus, while RAM does not incorporate shear mixing by impeller action into the mixing material, it does introduce a velocity profile of micro-mixing and bulk-mixing zones. Initially,

this profile is from frictional forces between particles, but as the system evolves into a paste and then a suspension, the velocity profile becomes a moving fluid, moving at an acceleration up to 100 times gravitational acceleration. Therefore, it is conceivable that the RAM results presented here are due to an increase in hydrate kinetics and change in physical and chemical microstructure. More work will need to be completed to confirm this qualitative reasoning. However, it is sufficing to say the RAM mixer can mix UHPC at high enough energies that change its microstructural development compared to a standard table top paddle mixer.

6. Conclusions

The works presented in this research offer a qualitative study of acoustic resonance mixing. The LabRAM by Resodyn Acoustic Technology® is a mixer that relies on reciprocal agitation movement rather than mechanical impeller or paddle agitation. In this study this mixer was used to mix ultra-high performance concrete. The following conclusions can be drawn:

- RAM mixing does not have a tool that directly interacts with the mixing medium. This makes it an attractive mixing device as it reduces the cost of wear and tear of the mixing device. Furthermore, the non-direct mixing action could be beneficial in cases where the interaction of the mixing tool and the mixing medium is an important parameter to consider, such as the case with fiber containing materials where the fibers can be bent from the mixing tool.
- RAM mixing is meant to operate at the system's resonance frequency. Thus, the main parameters that affect the final mixing outcome are the amplitude of the resonance acoustic pressure wave, the time of mixing, and the fill level of the vessel. More work will be needed to quantify the direct relationship of these parameters to the properties of the UHPC mix.
- Compared to a table top paddle mixer, RAM showed reduced flow and workability properties, but improved mechanical properties. A 30% increase in 3-day and 20% increase in 28-day mechanical properties were observed in UHPC specimens mixed with RAM. The improved mechanical properties support the understanding that there is more uniform mixing energy transmitted to the system during mixing which enhances cement hydration and reduces air voids.
- RAM can be considered qualitatively a high intensive mixer, yet further studies are needed to fully understand the mixing process of acoustic resonance mixing and its effects on cement and UHPC properties.
- Finally, this investigation demonstrates that this innovative mixing technology could have a place in concrete mixing technology.

Acknowledgements

This research has been supported by the Department of Homeland Security, the Department of Education, and the University of Connecticut. This material is also based upon work supported by the National Science Foundation under Grant No. 1454574. Additionally, the authors would like to acknowledge the support from the following companies: Lehigh White Cement Company, LafargeHolcim, Elkem Materials, Chryso, Resodyn Acoustic Technologies.

The publication of this document does not necessarily indicate approval or endorsement of the findings, opinions, conclusions, or recommendations either inferred or specifically expressed herein by the Department of Homeland Security, the Department of Education, or the United States Government.

References

[1] P. Richard, M. Cheyrezy, Composition of reactive powder concretes, Cem. Concr. Res. 25 (1995) 1501–1511.
[2] K. Wille, A.E. Naaman, G.J. Parra-Montesinos, Ultra high performance concrete with compressive strength exceeding 150 MPa (22 ksi): a simpler way, ACI Struct. Mater. J. 108 (2011) 46–54.
[3] S. Abbas, M.L. Nehdi, M.A. Saleem, Ultra-high performance concrete: mechanical performance, durability, sustainability and implementation challenges, Int. J. Concr. Struct. Mater. 10 (2016) 271–295.
[4] K. Wang, J. Hu, Use of a moisture sensor for monitoring the effect of mixing procedure on uniformity of concrete mixtures, J. Adv. Concr. Technol. 3 (2005) 371–383.
[5] D. Chopin, F. de Larrard, B. Cazacliu, Why do HPC and SCC require a longer mixing time?, Cem Concr. Res. 34 (2004) 2237–2243.
[6] D. Chopin, B. Cazacliu, Fd Larrard, R. Schell, Monitoring of concrete homogenisation with the power consumption curve, Mater. Struct. 40 (2007) 897–907.
[7] P. Jézéquel, V. Collin, Mixing of concrete or mortars: dispersive aspects, Cem. Concr. Res. 37 (2007) 1321–1333.
[8] J. Dils, G. De Schutter, V. Boel, Influence of mixing procedure and mixer type on fresh and hardened properties of concrete: a review, Mater. Struct. (2012) 1–11.
[9] P.N. Hiremath, S.C. Yaragal, Influence of mixing method, speed and duration on the fresh and hardened properties of reactive powder concrete, Constr. Build. Mater. 141 (2017) 271–288.
[10] K. Wille, K.J. Loh, Nano-engineering ultra-high performance concrete with multi-walled carbon nanotubes, Transp. Res. Rec.: J. Transp. Res. Board 2142 (2010) 119–126.
[11] S. Kawashima, Nanomodification of cementitious materials: fresh state and early age, March 2013.
[12] S. Chuah, Z. Pan, J.G. Sanjayan, C.M. Wang, W.H. Duan, Nano reinforced cement and concrete composites and new perspective from graphene oxide, Constr. Build. Mater. 73 (2014) 113–124.
[13] Z. Rong, W. Sun, H. Xiao, G. Jiang, Effects of nano-SiO2 particles on the mechanical and microstructural properties of ultra-high performance cementitious composites, Cem. Concr. Compos. 56 (2015) 25–31.
[14] K. Wille, C. Boisvert-Cotulio, Material efficiency in the design of ultra-high performance concrete, Constr. Build. Mater. 86 (2015) 33–43.
[15] M. Alkaysi, S. El-Tawil, Effects of variations in the mix constituents of ultra high performance concrete (UHPC) on cost and performance, Mater. Struct. 49 (2016) 4185–4200.
[16] E.L. Paul, V. Atiemo-Obeng, S.M. Kresta, Handbook of Industrial Mixing: Science and Practice, Wiley, 2004.
[17] P.M.C. Lacey, Developments in the theory of particle mixing, J. Appl. Chem. 4 (1954) 257–268.
[18] F.K. Saleh, C. Teodoriu, The mechanism of mixing and mixing energy for oil and gas wells cement slurries: a literature review and benchmarking of the findings, J. Nat. Gas Sci. Eng. 38 (2017) 388–401.
[19] D. Winslow, D. Liu, The pore structure of paste in concrete, Cem. Concr. Res. 20 (1990) 227–235.
[20] S. Diamond, Percolation due to overlapping ITZs in laboratory mortars? a microstructural evaluation, Cem. Concr. Res. 33 (2003) 949–955.
[21] G. Sant, C.F. Ferraris, J. Weiss, Rheological properties of cement pastes: a discussion of structure formation and mechanical property development, Cem. Concr. Res. 38 (2008) 1286–1296.
[22] D.P. Bentz, C.F. Ferraris, S.Z. Jones, D. Lootens, F. Zunino, Limestone and silica powder replacements for cement: early-age performance, Cem. Concr. Compos. 78 (2017) 43–56.
[23] R. Remus, C. Roessler, H. Ludwig, Power Ultrasound-assisted concrete production, in: Eleventh High Performance concrete (11th HPC) and the Second Concrete Innovation Conference (2nd CIC), 2017.
[24] J. Kamieński, R. Wójtowicz, Dispersion of liquid-liquid systems in a mixer with a reciprocating agitator, Chem. Eng. Process.: Process Intensif. 42 (2003) 1007–1017.
[25] R.H. Liu, J. Yang, M.Z. Pindera, M. Athavale, P. Grodzinski, Bubble-induced acoustic micromixing, Lab Chip 2 (2002) 151–157.
[26] J.G. Osorio, E. Hernández, R.J. Romañach, F.J. Muzzio, Characterization of resonant acoustic mixing using near-infrared chemical imaging, Powder Technol. 297 (2016) 349–356.
[27] K. Nagapudi, E.Y. Umanzor, C. Masui, High-throughput screening and scale-up of cocrystals using resonant acoustic mixing, Int. J. Pharm. 521 (2017) 337–345.
[28] D.H. Leung, D.J. Lamberto, L. Liu, E. Kwong, T. Nelson, T. Rhodes, et al., A new and improved method for the preparation of drug nanosuspension formulations using acoustic mixing technology, Int. J. Pharm. 473 (2014) 10–19.
[29] E. Batmaz, K.P. Sandeep, Integration of resonant acoustic® mixing into thermal processing of foods: a comparison study against other in-container sterilization technologies, J. Food Eng. 165 (2015) 124–132.
[30] ASTM C150/C150M-15, Standard Specification for Portland Cement, ASTM International, 2015.
[31] ASTM C494/C494M-15, Standard Specification for Chemical Admixtures for Concrete, ASTM International, 2015.
[32] S.L. Coguill Z, R. Martineau, Vessel Geometry and Fluid Properties Influencing Mix Behavior for Resonant Acoustic ® Mixing Processes, 2012.

[33] ResodynAcoustic Mixing I. RAM Technical White Paper, Resodyn Acoustic Mixers, Inc. 2009.
[34] J.T. Miller, S. Lubbering, P. Lucon, Mix Power, 2013 Resodyn Forum; Industrial Outcomes in Resonant Acoustic® Mixing, 2013.
[35] B. Cazacliu, In-mixer measurements for describing mixture evolution during concrete mixing, Chem. Eng. Res. Des. 86 (2008) 1423–1433.
[36] J. Moreno Juez, R. Artoni, B. Cazacliu, Monitoring of concrete mixing evolution using image analysis, Powder Technol. 305 (2017) 477–487.
[37] B. Cazacliu, J. Legrand, Characterization of the granular-to-fluid state process during mixing by power evolution in a planetary concrete mixer, Chem. Eng. Sci. 63 (2008) 4617–4630.
[38] B. Cazacliu, N. Roquet, Concrete mixing kinetics by means of power measurement, Cem. Concr. Res. 39 (2009) 182–194.
[39] K. Kovler, N. Roussel, Properties of fresh and hardened concrete, Cem. Concr. Res. 41 (2011) 775–792.
[40] P.F.G. Banfill, Rheology of fresh cement and concrete, Rheol. Rev. (2006) 61–130.
[41] V. Mechtcherine, E. Secrieru, C. Schroefl, Effect of superabsorbent polymers (SAPs) on rheological properties of fresh cement-based mortars — development of yield stress and plastic viscosity over time, Cem. Concr. Res. 67 (2015) 52–65.
[42] D.A. Williams, A.W. Saak, H.M. Jennings, The influence of mixing on the rheology of fresh cement paste, Cem. Concr. Res. 29 (1999) 1491–1496.
[43] D. Feys, R. Verhoeven, G. De Schutter, Evaluation of time independent rheological models applicable to fresh self-compacting concrete, Appl. Rheol. 17 (56244–1) (2007) 56244–56310.
[44] ASTM C109/C109M-13e1, Standard Test Method for Compressive Strength of Hydraulic Cement Mortars (Using 2-in. or [50-mm] Cube Specimens), ASTM International, 2013.
[45] A. Goldszal, J. Bousquet, Wet agglomeration of powders: from physics toward process optimization, Powder Technol. 117 (2001) 221–231.
[46] A.K. Chopra, Dynamics of Structures: Theory and Applications to Earthquake Engineering, Prentice Hall, 2012.
[47] J.A. Orban, P.A. Parcevaux, D.J. Guillot, Specific mixing energy: a key factor for cement slurry quality, 1986.
[48] A.P. Hibbert, D.J. Kellingray, B. Vidick, Effect of mixing energy levels during batch mixing of cement slurries, 1995.
[49] N. Roussel, C. Stefani, R. Leroy, From mini-cone test to Abrams cone test: measurement of cement-based materials yield stress using slump tests, Cem. Concr. Res. 35 (2005) 817–822.
[50] D. Han, R.D. Ferron, Influence of high mixing intensity on rheology, hydration, and microstructure of fresh state cement paste, Cem. Concr. Res. 84 (2016) 95–106.
[51] D. Han, R.D. Ferron, Effect of mixing method on microstructure and rheology of cement paste, Constr. Build. Mater. 93 (2015) 278–288.
[52] P. Juilland, A. Kumar, E. Gallucci, R.J. Flatt, K.L. Scrivener, Effect of mixing on the early hydration of alite and OPC systems, Cem. Concr. Res. 42 (2012) 1175–1188.